minerals

MDPI

Article

Modified Diglycolamide Resin: Characterization and Potential Application for Rare Earth Element Recovery

Junnile L. Romero [1,2,*], Carlito Baltazar Tabelin [1,3], Ilhwan Park [4], Richard D. Alorro [5,*], Joshua B. Zoleta [1,6], Leaniel C. Silva [1,3], Takahiko Arima [4], Toshifumi Igarashi [4], Takunda Mhandu [6], Mayumi Ito [4], Steffen Happel [7], Naoki Hiroyoshi [4] and Vannie Joy T. Resabal [1,3]

1 Department of Materials and Resources Engineering and Technology, Mindanao State University—Iligan Institute of Technology, Tibanga, Iligan City 9200, Philippines; carlito.tabelin@g.msuiit.edu.ph (C.B.T.); joshua.zoleta@g.msuiit.edu.ph (J.B.Z.); leaniel.silva@g.msuiit.edu.ph (L.C.S.); vanniejoy.resabal@g.msuiit.edu.ph (V.J.T.R.)
2 Helmholtz Zentrum Dresden Rossendorf, Helmholtz Institute Freiberg for Resource Technology, Chemnitzer Strasse 40, 09599 Freiberg, Germany
3 Research Institute of Engineering and Innovative Technology (RIEIT), Mindanao State University—Iligan Institute of Technology, Tibanga, Iligan City 9200, Philippines
4 Division of Sustainable Resources Engineering, Faculty of Engineering, Hokkaido University, Sapporo 060-8629, Japan; i-park@eng.hokudai.ac.jp (I.P.); takahiko_arima@eng.hokudai.ac.jp (T.A.); tosifumi@eng.hokudai.ac.jp (T.I.); itomayu@eng.hokudai.ac.jp (M.I.); hiroyosi@eng.hokudai.ac.jp (N.H.)
5 Western Australia School of Mines, Minerals, Energy and Chemical Engineering, Curtin University, Kent Street, Bentley, WA 6102, Australia
6 Division of Sustainable Resources Engineering, Graduate School of Engineering, Hokkaido University, Sapporo 060-8628, Japan; tjmhandu@gmail.com
7 International S.A.S., 3 Rue des Champs Géons ZAC de, L'Éperon, 35170 Bruz, France; shappel@triskem.fr
* Correspondence: romero.junnile01@gmail.com or j.romero@hzdr.de (J.L.R.); richard.alorro@curtin.edu.au (R.D.A.)

check for updates

Citation: Romero, J.L.; Tabelin, C.B.; Park, I.; Alorro, R.D.; Zoleta, J.B.; Silva, L.C.; Arima, T.; Igarashi, T.; Mhandu, T.; Ito, M.; et al. Modified Diglycolamide Resin: Characterization and Potential Application for Rare Earth Element Recovery. *Minerals* **2023**, *13*, 1330. https://doi.org/10.3390/min13101330

Academic Editors: Richmond K. Asamoah, Ahmet Deniz Baş, George Blankson Abaka-Wood, Kali Sanjay and Jonas Addai-Mensah

Received: 14 September 2023
Revised: 9 October 2023
Accepted: 11 October 2023
Published: 14 October 2023

Abstract: Rare earth elements (REEs) are crucial for green energy applications due to their unique properties, but their extraction poses sustainability challenges because the global supply of REEs is concentrated in a few countries, particularly China, which produces 70% of the world's REEs. To address this, the study investigated TK221, a modified extraction chromatographic resin featuring diglycolamide (DGA) and carbamoyl methyl phosphine oxide (CMPO), as a promising adsorbent for REE recovery. The elemental composition and functional groups of DGA and CMPO on the polystyrene-divinylbenzene (PS-DVB) support of TK221 were confirmed using scanning electron microscopy with energy dispersive X-ray spectroscopy (SEM-EDX), attenuated total reflectance Fourier transform infrared spectroscopy (ATR-FTIR), and X-ray photoelectron spectroscopy (XPS). The adsorption kinetics of neodymium (Nd), yttrium (Y), cerium (Ce), and erbium (Er) followed the pseudo-second-order kinetic model and Langmuir isotherm, indicating monolayer chemisorption. Furthermore, iron (Fe) adsorption reached apparent equilibrium after 360 min, with consistent Fe adsorption observed at both 360 min and 1440 min. The inclusion of Fe in the study is due to its common presence as an impurity in most REE leachate solutions. The Fe adsorption isotherm results are better fitted with the Langmuir isotherm, implying chemisorption. Maximum adsorption capacities (q_{max}) of the resin were determined as follows: Nd (45.3 mg/g), Ce (43.1 mg/g), Er (35.1 mg/g), Y (15.6 mg/g), and Fe (12.3 mg/g). ATR-FTIR analysis after adsorption suggested that both C=O and P=O bands shifted from 1679 cm^{-1} to 1618 cm^{-1} and 1107 cm^{-1} to 1142 cm^{-1} for Y, and from 1679 cm^{-1} to 1607 cm^{-1} and 1107 cm^{-1} to 1135 cm^{-1} for Ce, implying possible coordination with REEs. These results suggest that TK221 has a huge potential as an alternative adsorbent for REE recovery, thus contributing to sustainable REE supply diversification.

Keywords: rare earth elements; extraction chromatography; ion-exchange resin; adsorption; critical metals

1. Introduction

The Rare-Earth Elements (REEs), a group of 17 elements exhibiting similar chemical properties, have become vital in the last 30 years for the advancement of renewable energy and clean storage technologies owing to their unique magnetic, phosphorescent, and catalytic properties [1–3]. In 3 MW wind turbines, for example, 3 tons of REEs are needed [4], while in electric vehicles (EVs), REEs like neodymium (Nd), praseodymium (Pr), samarium (Sm), and dysprosium (Dy) are used in high efficiency and strong permanent magnets [2,5,6]. In 2012, the demand for Dy and Nd for the next 25 years was projected to increase by at least 700% and 2600%, respectively [7]. This situation is a supply security risk due to the inherent scarcity of REEs, which was further complicated because the maximum annual primary material demands for Dy and Nd exceeded the current production volumes by a factor of 3 to 9 and 7 to 35, respectively [8]. Exacerbating this problem is that China, the primary exporter of REEs (78%) from primary resources, imposed export restrictions, citing increasing domestic REE requirements and environmental concerns related to REE mining, processing, and extraction [2,9–11].

Generally, extraction of REEs involves comminution, physical separation, leaching, and solvent extraction [12]. Subsequent refinement involves solvent extraction for purification [13]. REE processing, according to Zapp (2022), involves significant chemical use, which is particularly noticeable during the solvent extraction stage. This process typically requires mixer, settler, stripping, and washing stages, further amplifying the chemical demand [14]. Additionally, the life cycle assessment of REE production highlighted the environmental challenge of managing and disposing of large quantities of chemical-bearing wastewater used in the beneficiation, extraction, and separation processes. Another challenge is that REE processing generates substantial amounts of tailings, which require proper disposal to limit their negative environmental impacts [14]. Additionally, the majority of REE-bearing ores have low REE contents and contain various metals with similar physicochemical properties as REEs that interfere with solvent extraction [15–17]. A study by Larochelle et al. (2002), for example, reported that calcium (Ca), aluminum (Al), and zinc (Zn) directly compete with REEs during the extraction and separation process [18]. As an alternative to solvent extraction, the use of extraction chromatographic resins has gained popularity in recent years because they combine the excellent selectivity and high efficiency of solvent extraction and simplicity of ion exchange [19]. These resins are prepared by incorporating functionalized ligands onto solid support like porous polymers, and selections of a selective extractant and excellent support are both crucial for the resins to be effective [19,20].

Dialkyl resins (LN) [21] resin is a commercial resin available from Triskem International, commonly used for cation, lanthanide, and radium separation, and light rare-earth element determination; however, it is problematic for coal fly ash REE leachate purification due to its high-capacity factor for impurities such as Fe, Al, Si, and Ca. Similarly, rare earth (RE) [21] resin, a commercial resin available from Triskem International, is widely used for the group separation of REEs and has a similar limitation due to its high-capacity factor for Fe [22,23]. Other commercial resins, TK 211/212/213 resins available from Triskem International, have high selectivity for specific lanthanide pairs, but their small particle size makes them difficult to handle in a chromatographic column [24]. In 2005, Horwitz et al. (2005) introduced the diglycolamide (DGA) resin, a novel material containing the DGA ligand, a well-known lanthanide extractant with a high-quality chelating tridentate capacity [25–28]. Follow-up works using the DGA resin reported an increase in the distribution coefficient of trivalent lanthanides with increasing nitric acid (HNO_3) or hydrochloric acid (HCl) concentration [29,30]. Moreover, octyl(phenyl)-N,N-diisobutyl carbamoylmethyl phosphine oxide (CMPO) has been found to extract REEs [28,31,32]. Based on these developments, Triskem has developed a combination of the extractants DGA and CMPO into a new chromatographic resin called TK221. Although this resin has been applied in the pharmaceutical industry and in the study of actinide concentration in water [33] and

scandium extraction [34], its utilization for bulk extraction of REEs from leachates has not yet been explored.

Thus, this study aims to characterize the particle size, chemical composition, and functional groups of TK221, as well as determine the adsorption properties of Nd, Ce, Er, and Fe on this resin. The first objective was achieved via attenuated total reflectance Fourier transform infrared spectroscopy (ATR-FTIR), X-ray photoelectron spectroscopy (XPS), and scanning electron microscopy with energy dispersive X-ray spectroscopy (SEM-EDX) while the second objective was attained by performing kinetic rate law and adsorption isotherm experiments.

2. Experimental

2.1. Materials

In this study, high purity Nd(III) (0.99–1.01 mg/mL), Y(III) (0.99–1.01 mg/mL), Ce(III) (0.99–1.01 mg/mL), Er(III) (0.99–1.01 mg/mL), and Fe(III) (990–1010 mg/L) standard solutions for inductively coupled plasma atomic emission spectroscopy (ICP-AES), which is dissolved in 1 M HNO_3, purchased from FUJIFILM Wako Pure Chemical Corporation (Chuo-ku, Osaka, Japan) were used. The selection of Nd, Y, and Er was based on their economic value, while Ce and Fe were included due to their frequent occurrence as coexisting REE impurities, respectively. The selection of 3 M HCl was based on both previous works and the resin manufacturer's recommendation, which suggests that adsorption is likely to occur at this HCl concentration [21]. The TK221 chromatographic resin was provided by Triskem International SAS (Bruz, Bretagne, France), which can typically be regenerated up to 10 times as indicated by the manufacturer.

2.2. Characterization of TK221 Resin

To determine the functional groups present on the TK221 resin, ATR-FTIR and XPS were performed using an FT/IR-6200 HFV (Jasco Analytical Instruments, Japan) and JPS-9200 (JEOL Ltd., Ishikawa-cho Hachioji, Tokyo), respectively. The XPS instrument was equipped with a monochromatized Al Kα X-ray source operating at 100 W under ultrahigh vacuum (about 10^{-7} Pa). Narrow scan spectra of oxygen (O1s) and carbon (C1s) were obtained and corrected using the binding energy of adventitious carbon (285.0 EV). All XPS spectra were deconvoluted with XPSPEAK version 4.1 using a true Shirley background and a 20%–80% Lorentzian-Gaussian peak model [35]. In addition to XPS, the size distribution of the resin was determined using LASER diffraction (Microtrac® MT3300SX, Nikkiso Co., Ltd., Shibuya-ku, Tokyo, Japan) to ensure a representative sample for subsequent analysis. The morphology and elemental composition of TK221 were then determined using SEM-EDX (JSM-IT200, JEOL Co., Ltd., Musashino Akishima, Tokyo; Japan). The SEM-EDX analysis was conducted in BED-C mode with an accelerating voltage of 15 kV at 10,000 cps with a 1.0 ms time constant under ultrahigh vacuum, and the magnification used for the analysis was 430.

2.3. Batch Kinetic Adsorption Isotherm Tests (Single Element)

A series of single-element batch kinetic rate law experiments were conducted using individual stock solutions of Nd(III), Y(III), Ce(III), Er(III), and Fe(III) in 3 M HCl with concentrations of 93 mg/L, 137 mg/L, 126 mg/L, and 117 mg/L, and 477 mg/mL, respectively. The variation in feed concentration for each element was strategically implemented to ensure that the recovery remains at approximately 50%. This approach guarantees that the resin has an adequate quantity of metal ions available for adsorption. Furthermore, in practical applications, leachates derived from different sources contain a wide range of concentrations for various REEs.

For the adsorption test, 0.1 g of TK221 was soaked in 5 mL of 3 M HCl in a 50 mL Erlenmeyer flask for at least 12 h at room temperature to allow the resin to swell and increase its capacity. After swelling, 5 mL of the REE stock solution was added to the flask,

and the batch test was initiated by placing the flask in a water bath shaker at 25 °C and 120 rpm.

Samples were collected after 1, 3, 5, 10, 15, 30, 60, 180, 380, and 1440 min of contact time. The suspensions were then filtered through 0.45 µm syringe-driven filters (LMS Co., Ltd., Hongo, Bunkyo-ku, Tokyo, Japan), and the residual concentrations of Nd, Y, Ce, and Er were analyzed using ICP-AES (ICPE-9820, Shimadzu Corporation, Kyoto, Japan) (margin of error = ±2%).

To determine the equilibrium time and concentration of the REEs on the resin, the concentration of the aqueous phase was plotted against contact time, and the slope of the resulting line was used to calculate the rate constant. The data were fitted with the pseudo-first-order and pseudo-second-order kinetic rate law models. It is crucial to note the assumptions of both models, as follows: (1) adsorption occurs at specific sites, where no interaction occurs between the solutes adsorb; (2) the adsorption energy is independent of the surface coverage; (3) attainment of monolayer coverage on the adsorbent surface yields maximum adsorption; (4) the concentration of the solutes does not change; and (5) adsorption of the solutes is controlled by either pseudo-first-order and pseudo-second-order rate equation [36].

The pseudo-first-order can be expressed as:

$$q_t = q_e\left(1 - e^{-k_1 t}\right) \tag{1}$$

where:

k_1—is the rate constant of the pseudo-first-order adsorption
q_e—is the amount of solute adsorb at equilibrium
q_t—is the amount of solute adsorb at time t
t—is the contact time

The pseudo-second-order model can be expressed as:

$$q_t = (k_2 \times {q_e}^2)/(1 + k_2 \times t)$$

where:

k_2—is the rate constant of the pseudo-second-order adsorption
q_e—is the amount of solute adsorb at equilibrium
q_t—is the amount of solute adsorb at time t
t—is the contact time

The pseudo-second-order model can be rearranged into a linear form:

$$t/q_t = 1/(k_2 \times {q_e}^2) + t/q_t \tag{2}$$

The equilibrium time was determined from the intersection of the equilibrium line with the time axis, which represented the time when the concentration of REEs on the resin reached a steady state. To ensure reproducibility and reliability of the results, the experiments at 3, 5, 10, and 15 min of all REEs were replicated three times.

2.4. Single Element Batch Isotherm Adsorption Tests

A series of single-element batch isotherm adsorption experiments were conducted using individual solutions of Nd(III), Y(III), Ce(III), Er(III) and Fe(III) in 3 M HCl with concentrations ranging from 93.2 mg/L to 846 mg/L, 87.9 mg/L to 718 mg/L, 126 mg/L to 802 mg/L, 124 mg/L to 813 mg/L, and 30.4 mg/L to 502 mg/L, respectively. Before the adsorption tests, the resin was allowed to swell using 3 M HCl (2–5 mL) as outlined previously. After swelling, 5–8 mL of the REE solution was added into the flask, with the volume of solution dependent on the swelling solution used to ensure a total volume of 10 mL. The pH of the solution was measured before and after adsorption.

The batch adsorption test was initiated by placing the flask in a thermostat water bath shaker at 25 °C and 120 rpm. The samples were collected after reaching apparent

equilibrium at 360 min, which was determined in the batch kinetic adsorption tests. The filtrates were collected by filtration, and residual REE concentration was analyzed using ICP-AES. Meanwhile, the loaded resin was collected, washed thoroughly with deionized water, dried in a vacuum oven at 40 °C, and analyzed using SEM-EDX and ATR-FTIR.

The adsorption data were fitted with Langmuir and Freundlich isotherms to determine the adsorption mechanisms of REEs onto TK221, and the best R-squared value was used to select the most appropriate isotherm model.

The Langmuir isotherm assumes single monolayer adsorption and is given by:

$$q = (q_{max} \times K_L) \times \left(\frac{C}{1 + K \times C}\right)$$

where:

q—is the amount of solutes adsorbed per unit weight of adsorbent

C—is the equilibrium concentration of the solutes in solution

q_{max}—is the maximum amount of solutes that can be adsorbed per unit weight of adsorbent

K_L—is the Langmuir constant related to the energy of adsorption

The linear form of the Langmuir isotherm equation is:

$$\frac{1}{q} = \left(\frac{1}{q_{max}}\right) + \left(\frac{1}{K_L \times q_{max}}\right) \times 1/C \quad (3)$$

The Freundlich isotherm assumes that multilayer adsorption occurs and is given by:

$$q = K_f \times C^{\frac{1}{n}}$$

where:

q—is the amount of solute adsorb per unit weight of adsorbent

C—is the equilibrium concentration of the solutes in solution

K_f—is the Freundlich constant related to the adsorption capacity

n—is the Freundlich exponent related to the adsorption intensity

The linear form of the Freundlich isotherm equation is:

$$\ln(q) = \ln\left(K_f\right) + \left(\frac{1}{n}\right) \times \ln(C) \quad (4)$$

3. Results and Discussion

3.1. Characterization of TK221: Insights from SEM-EDX, Microtrac, ATR-FTIR, and XPS

The elemental mapping shown in Figure 1a indicates an even distribution of main elements, including Carbon (C), Nitrogen (N), Phosphorus (P), and Oxygen (O) throughout the resin. The strong EDX signals of N and P confirmed the presence of DGA and CMPO on the surface of TK221, and their uniform distribution suggests that the extraction capabilities of TK221 would be consistent and reliable.

The particle size distribution of the resin is shown in Figure 1b, and it is mainly between 100 μm and 200 μm. Compared to traditional chromatographic resins prepared with pure polymer matrix in the particle size of 0.3–3 mm, this new type of extraction resin has a smaller particle size, which can result in faster kinetics, higher strength, and better flowability in the packed column [24]. These characteristics are important for improving the efficiency of the extraction process and reducing the amount of solvent used. However, it should be noted that further testing is required to fully understand the impact of the smaller particle size on the resin's performance and extraction efficiency.

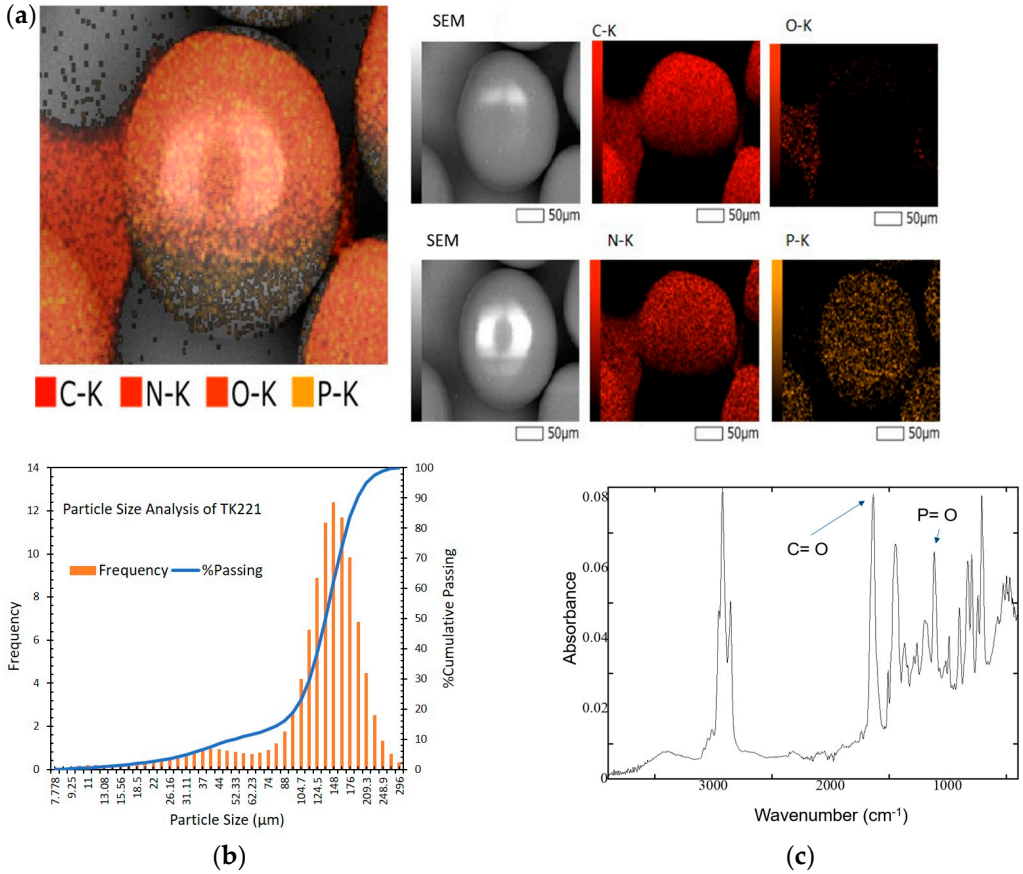

Figure 1. (**a**) Photomicrograph and elemental mapping of fresh TK221, (**b**) particle size distribution of fresh TK221, (**c**) ATR-FTIR spectrum of fresh TK221.

Figure 1c displays the ATR-FTIR analysis of fresh TK221, and Table 1 indicate the presence of several important functional groups. The absorption band between 3600–3400 cm^{-1} corresponds to O-H vibrations of water [20,37,38], while that at 2950–2850 cm^{-1} indicates the presence of C-H vibrations of TODGA [20,29,39,40]. The IR peak at 1700–1600 cm^{-1} suggests the presence of C=O vibrations of Amide I and CMPO [20,29,39,40], and the 1570–1470 cm^{-1} absorption band depicts the C-N vibrations of Amide II [29]. Meanwhile, the IR peak at 1200–1100 cm^{-1} shows the presence of P=O vibrations of CMPO [39,41], while that at 900–700 cm^{-1} is assigned to C-H vibrations of PS-DVB [37].

Table 1. ATR-FTIR peak assignments of fresh TK221.

Wavelength (cm^{-1})	Corresponding Chemical Structure	Reference
3600–3400	O-H of water	[20,37]
2950–2850	C-H of TODGA *	[20,29,39,40]
1700–1600	C=O of Amide I and CMPO	[20,29,39,40]
1570–1479	C-N of Amide II	[29]
1200–1100	P=O of CMPO	[39,41]
900–700	C-H of PS-DVB	[37]

* Note: TODGA means tetraoctyl diglycolamide.

Figure 2b displays the C(1s) spectra of TK221, which was deconvoluted into three peaks assigned to C-O/C-C, amide, and C=O, as shown in Table 2. The peak at binding energy (BE) of 285.96 corresponded to the presence of C-O/C-N of DGA and the C=C of PS-DVB [20,40,42]. Additionally, the peak at a BE of 286.87 indicates the presence of the

amide group of DGA [40,42]. Lastly, the peak at a BE of 288.68 implies the presence of the C=O group of DGA [20,42].

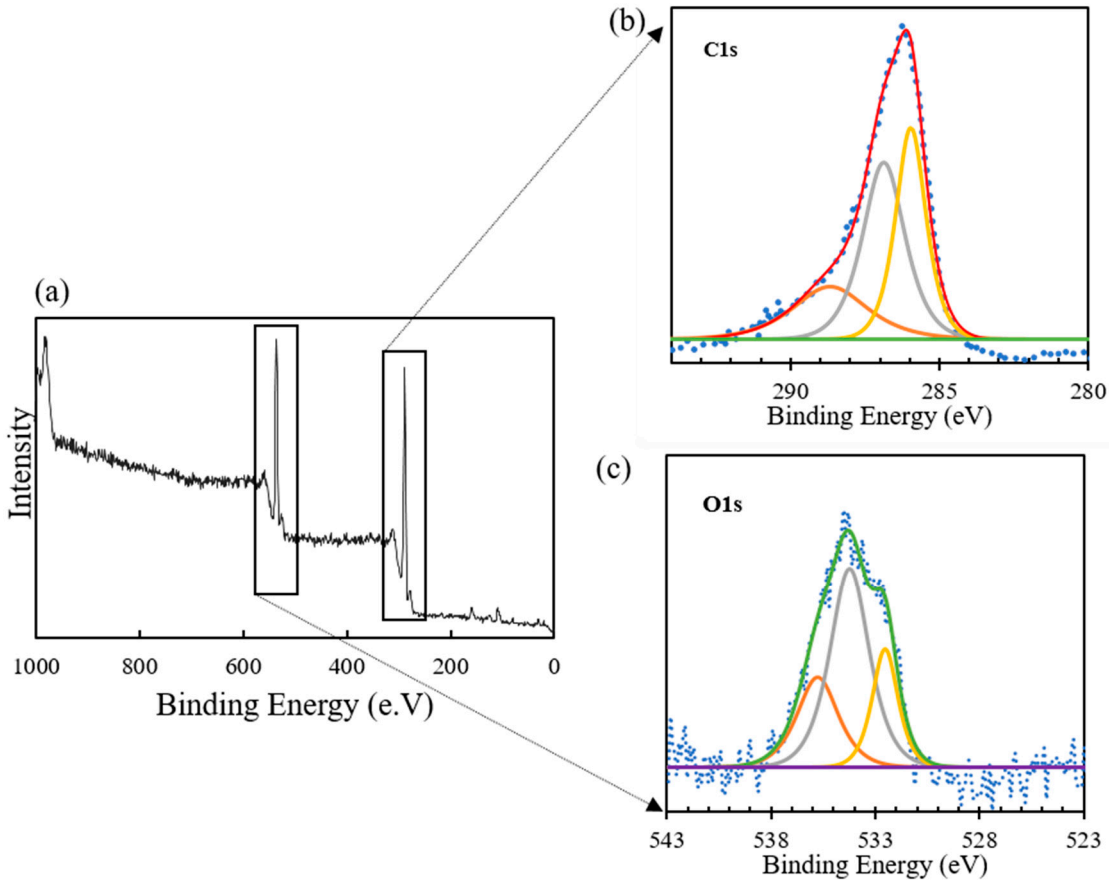

Figure 2. (**a**) XPS wide scan of fresh TK221, (**b**) XPS narrow scan spectrum of fresh TK221 at C(1s), and (**c**) XPS narrow scan spectrum of fresh TK221 at O(1s).

Table 2. XPS data and chemical states of fresh TK221 resin.

Spectral Peak	Chemical State	Binding Energy (eV)	
		This Study	Reference
O(1s)	P=O/C=O	532.02	[43]
O(1s)	C-O	534.22	[43]
O(1s)	Chemically bonded water	535.75	[41,44,45]
C(1s)	C-O/C-C	285.96	[20,40,42]
C(1s)	Amide	286.87	[20,40,42]
C(1s)	C=O	288.67	[20,42]

Figure 2c shows the O(1s) spectrum of TK221, which was deconvoluted into three peaks assigned to P=O/C=O, C-O, and chemically adsorbed H_2O, as shown in Table 2. The peak at a BE of 532.02 corresponded to the P=O of CMPO and the C=O of the DGA [43]. Additionally, the peak at BE of 534.22 indicates the presence of C-O of DGA [43]. The peak at a BE of 535.75 implies the presence of chemically adsorbed H_2O [41,44,45], reaffirming the results of the ATR-FTIR analysis. Overall, the XPS analysis of O(1s) confirms the composition of TK221 and provides valuable insight into the surface chemistry of the resin.

Taken together, the SEM-EDX analysis revealed that TK221, a resin comprised of tributyl phosphate (TRU) and diglycolamide (DGA) resins coated onto a polystyrene-divinylbenzene (PS-DVD) inert support, contains REE extractants CMPO and DGA. Further, the ATR-FTIR and XPS peaks indicate the presence of TODGA and CMPO in TK221 coated

on PS-DVB. The presence of these functional groups is significant, as they are responsible for the extraction properties of the resin. The identification of these functional groups using ATR-FTIR and XPS analysis supports the use of TK221 in metal ion extraction and other related applications. However, further testing and analysis will be necessary to fully understand the performance of TK221 in various extraction processes.

3.2. Adsorption Kinetics

The adsorption kinetics of Nd(III), Ce(III), Er(III), and Y(III) on TK221 at room temperature were investigated, and the results are shown in Figure 3a,b. The equilibrium adsorption capacity was found to be 7.65 mg Nd/g, 9.90 mg Ce/g, 12.4 mg Er/g, and 8.99 mg Y/g, respectively, which were reached after 360 min of contact time. The experimental data were fitted with pseudo-first-order and pseudo-second-order kinetic models, and the fitting parameters obtained by linear fitting were listed in Table 3. The correlation coefficients (R2) of the pseudo-second-order model were found to be 1.00 for all the studied REEs, indicating that adsorption predominantly occurred via chemisorption. Notably, for Fe, the amount adsorbed and recovery at 360 min suggest a similar equilibrium time with the REEs, as seen in Table 4.

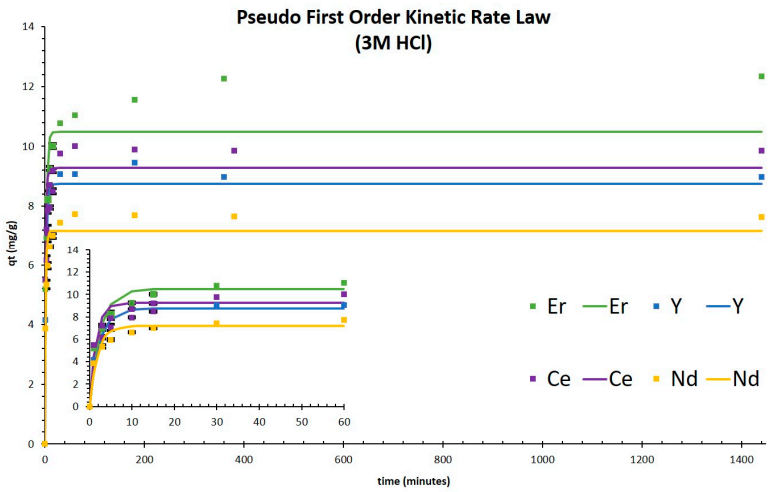

(**a**)

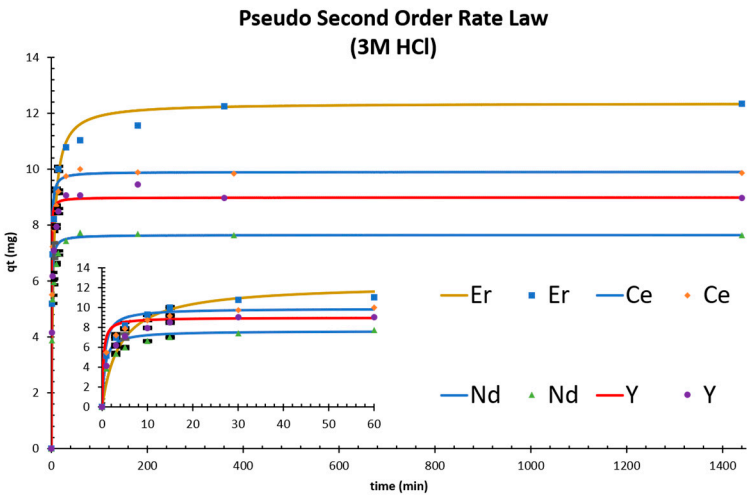

(**b**)

Figure 3. (**a**) pseudo-first-order kinetic rate law fitting for Nd, Ce, Er, and Y adsorption, and (**b**) pseudo-second-order kinetic rate law fitting for Nd, Ce, Er, and Y adsorption.

Table 3. Kinetic rate law fitting parameters for Nd, Ce, Er, and Y on TK221.

Element	Pseudo-First-Order			Pseudo-Second-Order		
	k1	Qe	R^2	k2	Qe	R^2
Nd	0.539	7.18	0.949	0.220	7.65	1.00
Ce	0.661	9.27	0.945	0.189	9.90	1.00
Er	0.403	10.48	0.903	0.021	12.4	1.00
Y	0.440	8.75	0.964	0.409	8.99	1.00

Table 4. Fe adsorption and recovery at 360 and 1440 min.

Element	Adsorption (mg/g)		%Recovery	
	360 min	1440 min	360 min	1440 min
Fe	11.1	10	23	21

3.3. Adsorption Isotherm

Figure 4a,b depict the adsorption isotherms of Nd(III), Ce(III), Er(III), Y(III), and Fe(III) at room temperature to TK221. REE adsorption increased with the target ion concentration of the feed solution, resulting in higher adsorption capacities, consistent with previous experiments that used DGA [20]. The equilibrium adsorption data were fitted and analyzed using Langmuir and Freundlich isotherms, and the results are illustrated in Table 5. The Langmuir isotherm exhibited a higher correlation coefficient than the Freundlich isotherm, indicating that the recovery of Nd(III), Ce(III), Er(III), Y(III), and Fe(III) mainly occurred via homogenous monolayer adsorption. The saturated adsorption capacities (q_{max}) were found to be 45.2 mg Nd/g, 43.1 mg Ce/g, 35.1 mg Er/g, 15.6 mg Y/g, and 12.3 mg Fe/g. Values of the Langmuir coefficient (K_L) are related to the relative affinity of the functional groups towards the target ions [46–48]. This means that when the five elements coexist in solution, the TK221 resin will preferentially extract the target elements in the following order: Er > Y > Fe > Nd > Ce (Table 5).

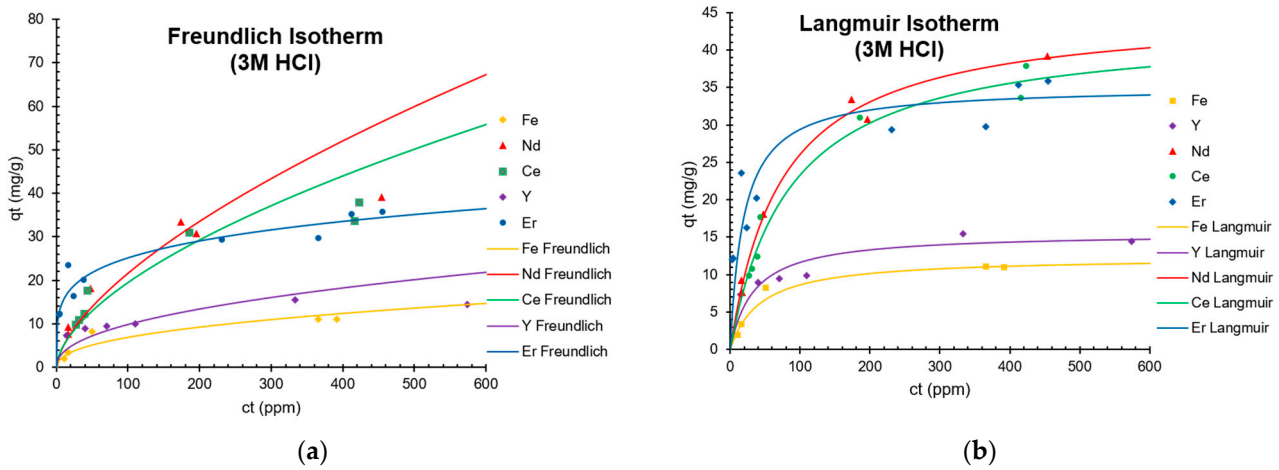

(**a**) (**b**)

Figure 4. (**a**) Freundlich Isotherm fitting Nd, Ce, Er, Y, and Fe and (**b**) Langmuir Isotherm fitting Nd, Ce, Er, Y, and Fe.

These results also align with hard and soft acid-base (HSAB) theory, where both amide and phosphine oxide functional groups are considered "soft" bases [49,50], so they have a higher affinity towards "soft acids". In this study, the use of 3 M HCl, while not strong enough to alter the charge states of the ions, allowed us to consider their relative charge densities as a primary factor in determining their behavior. Based on this analysis, we can establish an order of increasing charge density among the studied elements: Ce > Nd > Er

> Y > Fe. This ordering implies that REEs possess a higher degree of softness compared to Fe, which is a significant finding in understanding their chemical behavior.

Table 5. Adsorption isotherms fitting parameters of TK221 for Nd, Ce, Er, Y, and Fe.

Element	Freundlich Isotherm			Langmuir Isotherm			
	k_F	n	R^2	k_L	q_{max}	R^2	T-Test $t_{0.995}$
Nd	1.17	2.25	0.98	0.014	45.2	0.995	significant
Ce	1.31	1.70	0.96	0.012	43.1	0.986	significant
Er	8.78	4.51	0.90	0.052	35.1	0.985	significant
Y	1.27	2.25	0.92	0.030	15.6	0.989	significant
Fe	0.994	4.51	0.96	0.023	12.3	0.996	significant

The ability of TK221 resin to selectively extract REEs from aqueous solutions suggests that it is a promising alternative to solvent extraction, but pretreatment steps to concentrate REEs or remove interfering ions like Fe may be necessary for improved performance and selectivity. Moreover, the use of TK221 as an adsorbent for REE removal may offer several advantages over other methods, such as its low cost, ease of regeneration, and potential for scalability. Overall, as shown in Table 6, these findings highlight the potential of TK221 as a highly effective and practical adsorbent for the removal of REEs from aqueous solutions and may contribute to the development of efficient and sustainable methods for REE recovery.

Table 6. Comparison of Nd, Ce, Er, Y, and Fe adsorption capacity of TK221 with previous works.

Reference	Adsorbent Resin	pH	Element	q_{max} (mg/g)
This study	TK221	−0.264–−0.325	Nd	45.2
		−0.230–−0.327	Ce	43.1
		−0.274–−0.313	Er	35.1
		−0.116–−0.202	Y	15.6
		−0.116–0.102	Fe	12.3
[20]	TODGA-modified macroporous silica-polymer-based	-	Zr	20.0
		-	Sc	8.16
[29]	TEHDGA impregnated resin	-	La	1.31
		-	Nd	0.53
		-	Y	1.45
		-	Er	1.3
[51]	Functionalized Cr-MIL-101	2–6	La	37.4
		2–6	Ce	49.0
		2–6	Nd	70.9
		2–6	Sm	72.7
		2–6	Gd	90.0

Note: "-" means "not evaluated".

3.4. Adsorption Mechanism

To elucidate the possible bonding mechanism between the resin and the REEs, the residue of the highest point in the adsorption batch test was characterized using SEM-EDX and ATR-FTIR, as shown in Figure 5.

The SEM-EDX and ATR-FTIR results suggest that yttrium forms a complex with CMPO, while chlorine acts as a counter ion stabilizing the complex of the ligand and REEs. The complex formation of Ce with DGA and CMPO is also supported by the literature. The equilibrium reaction for metal ion extraction using DGA is shown in Equation (5)

$$\begin{gathered}\text{Reactants} \rightleftharpoons \text{Products} \\ M^{n+}{}_{(aq)} + nA^{-}{}_{(aq)} + yL_{(org)} \rightleftharpoons M(A)_{(n)} \cdot yL_{(org)}{}^{-} / (M_{(hyd)} \cdot L_{(y)}{}^{(n+1)} \cdot nA^{-})_{org}\end{gathered} \quad (5)$$

Furthermore, it is observed that CMPO and DGA have similar behavior in the extraction of Am(III) [52]. ATR-FTIR analysis of the loaded resin shows that the peaks of C=O and P=O have shifted, indicating that they have coordinated with REEs after the adsorption of Y and Ce. The IR peak at 3279 cm^{-1} was attributed to the O-H stretching of water, while the peak at 2365 cm^{-1} was assigned to the Cl^-. Overall, these results suggest that the bonding mechanism between the resin and the REEs involved the coordination of C=O and P=O groups with the REEs, as well as the formation of complexes with CMPO and counter ions such as Cl^-.

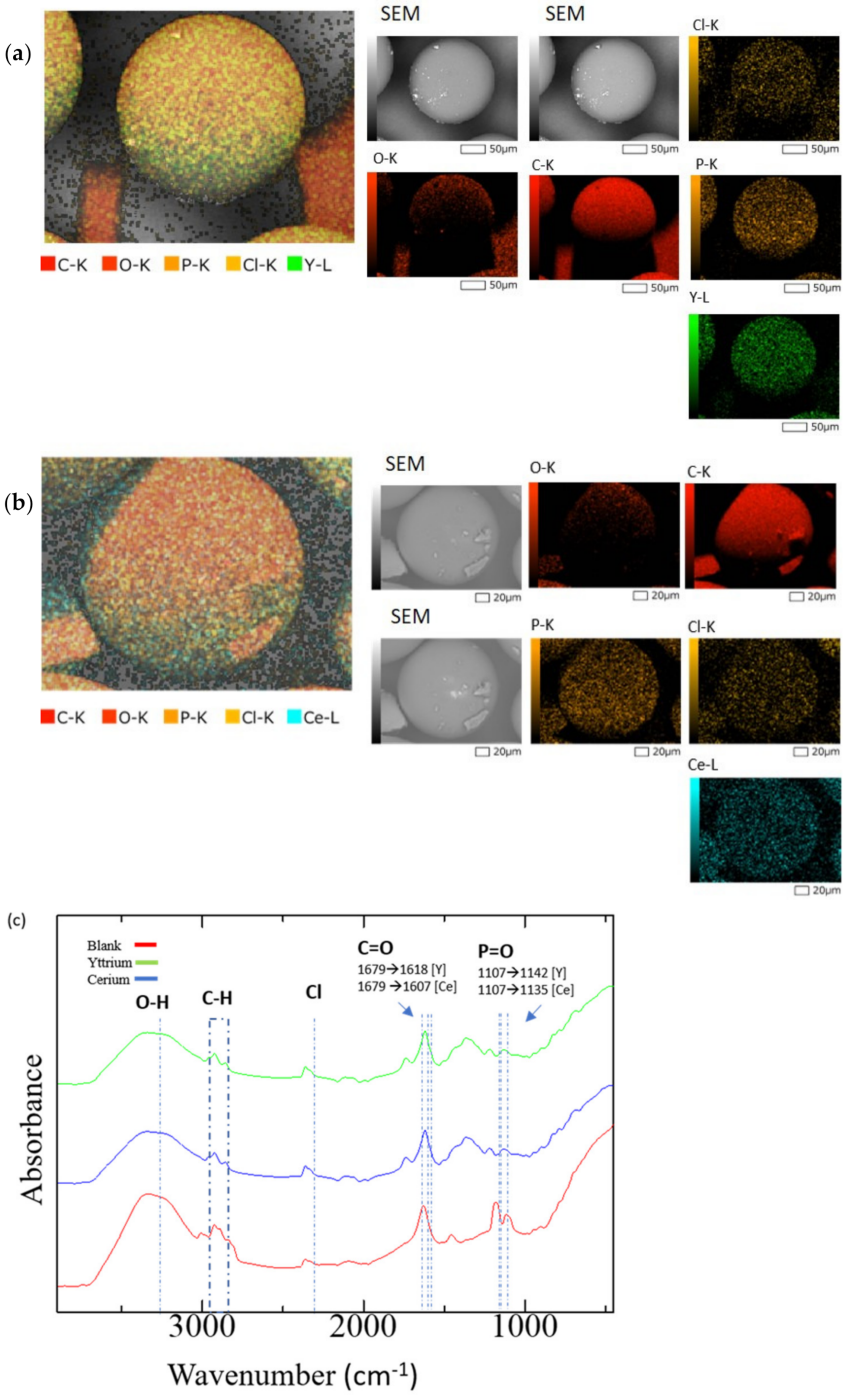

Figure 5. (**a**) Elemental mapping of after adsorption of TK221 resin loaded with yttrium, (**b**) Elemental Mapping of after adsorption of TK221 resin loaded with cerium, (**c**) ATR-FTIR analysis of TK221 of blank (red), loaded with yttrium (green), and loaded with cerium (blue).

4. Conclusions

TK221 holds substantial promise for effectively recovering rare earth elements (REEs) from matrix solutions. The characterization results obtained using SEM-EDX, ATR-FTIR, and XPS analyses confirm the presence of crucial functional groups (such as C=O, P=O, C-O) associated with DGA and CMPO, facilitating the adsorption of metal ions. Furthermore, we achieved adsorption equilibrium within a mere 360 min; notably, for Nd, Ce, Y, and Er, the data aligned well with the pseudo-second-order model, highlighting chemisorption as the primary adsorption mechanism with a maximum R^2 value of 1.00. In the investigation of Nd, Ce, Y, Er, and Fe, the Langmuir adsorption isotherm model provided an excellent fit, revealing a maximum adsorption capacity (q_{max}) of 45.2 mg/g for Nd. These results emphasize TK221's potential as a highly effective adsorbent for REE recovery from matrix solutions. However, taking proactive measures to address factors that influence the adsorption process remains imperative. Furthermore, the applications of this resin extend beyond REE recovery, encompassing fields like environmental remediation and resource recovery.

Author Contributions: Conceptualization, J.L.R. and C.B.T.; methodology, J.L.R. and C.B.T.; software, J.B.Z.; validation, J.L.R., C.B.T., I.P. and T.A.; formal analysis, J.L.R., I.P. and C.B.T.; investigation J.L.R., T.M. and J.B.Z.; resources, T.I., M.I., R.D.A. and S.H.; data curation, J.L.R., C.B.T. and J.B.Z.; writing—original draft preparation, J.L.R.; writing—review and editing, J.L.R., C.B.T., T.A. and I.P.; visualization, J.L.R., I.P. and C.B.T.; supervision, V.J.T.R., C.B.T., R.D.A., I.P. and N.H.; project administration, V.J.T.R.; funding acquisition, V.J.T.R. and L.C.S. All authors have read and agreed to the published version of the manuscript.

Funding: This research was funded by the Department of Science and Technology through the Engineering Research and Development for Technology (ERDT) for the MS scholarship granted to Junnile Romero and the APC was funded by Curtin University.

Data Availability Statement: No new data were created or analyzed in this study. Data sharing is not applicable to this article.

Acknowledgments: The authors wish to acknowledge the support provided by Triskem International for their generous provision of the TK221 resin used in this research.

Conflicts of Interest: The authors declare no conflict of interest.

References

1. Balaram, V. Rare earth elements: A review of applications, occurrence, exploration, analysis, recycling, and environmental impact. *Geosci. Front.* **2019**, *10*, 1285–1303. [CrossRef]
2. Van Gosen, B.S.; Verplanck, P.L.; Long, K.R.; Gambogi, J.; Seal, R.R. *How Do We Use the Rare-Earth Elements?* U.S. Geological Survey: Reston, VA, USA, 2014. [CrossRef]
3. Patil, A.B.; Paetzel, V.; Struis, R.P.W.J.; Ludwig, C. Separation and Recycling Potential of Rare Earth Elements from Energy Systems: Feed and Economic Viability Review. *Separations* **2022**, *9*, 56. [CrossRef]
4. Tabelin, C.B.; Park, I.; Phengsaart, T.; Jeon, S.; Villacorte-Tabelin, M.; Alonzo, D.; Yoo, K.; Ito, M.; Hiroyoshi, N. Copper and critical metals production from porphyry ores and E-wastes: A review of resource availability, processing/recycling challenges, socio-environmental aspects, and sustainability issues. *Resour. Conserv. Recycl.* **2021**, *170*, 105610. [CrossRef]
5. Dahan, A.M.E.; Alorro, R.D.; Pacaña, M.L.C.; Baute, R.M.; Silva, L.C.; Tabelin, C.B.; Resabal, V.J.T. Hydrochloric Acid Leaching of Philippine Coal Fly Ash: Investigation and Optimisation of Leaching Parameters by Response Surface Methodology (RSM). *Sustain. Chem.* **2022**, *3*, 76–90. [CrossRef]
6. Coey, J.M.D. Perspective and Prospects for Rare Earth Permanent Magnets. *Engineering* **2020**, *6*, 119–131. [CrossRef]
7. Alonso, E.; Sherman, A.M.; Wallington, T.J.; Everson, M.P.; Field, F.R.; Roth, R.; Kirchain, R.E. Evaluating rare earth element availability: A case with revolutionary demand from clean technologies. *Environ. Sci. Technol.* **2012**, *46*, 3406–3414. [CrossRef]
8. Junne, T.; Wulff, N.; Breyer, C.; Naegler, T. Critical materials in global low-carbon energy scenarios: The case for neodymium, dysprosium, lithium, and cobalt. *Energy* **2020**, *211*, 118532. [CrossRef]
9. Kim, R.; Cho, H.; Han, K.N.; Kim, K.; Mun, M. Optimization of acid leaching of rare-earth elements from mongolian apatite-based ore. *Minerals* **2016**, *6*, 63. [CrossRef]
10. Mancheri, N.A.; Sprecher, B.; Bailey, G.; Ge, J.; Tukker, A. Effect of Chinese policies on rare earth supply chain resilience. *Resour. Conserv. Recycl.* **2019**, *142*, 101–112. [CrossRef]
11. El Ouardi, Y.; Virolainen, S.; Mouele, E.S.M.; Laatikainen, M.; Repo, E.; Laatikainen, K. The recent progress of ion exchange for the separation of rare earths from secondary resources—A review. *Hydrometallurgy* **2023**, *218*, 106047. [CrossRef]

12. Gupta, C.K.; Krishnamurthy, N. (Nagaiyar) Krishnamurthy. In *Extractive Metallurgy of Rare Earths*; CRC Press: Boca Raton, FL, USA, 2005.
13. Park, I.; Kanazawa, Y.; Sato, N.; Galtchandmani, P.; Jha, M.K.; Tabelin, C.B.; Jeon, S.; Ito, M.; Hiroyoshi, N. Beneficiation of low-grade rare earth ore from Khalzan Buregtei deposit (Mongolia) by magnetic separation. *Minerals* **2021**, *11*, 1432. [CrossRef]
14. Zapp, P.; Schreiber, A.; Marx, J.; Kuckshinrichs, W. Environmental impacts of rare earth production. *MRS Bull.* **2022**, *47*, 267–275. [CrossRef]
15. Li, C.; Ramasamy, D.L.; Sillanpää, M.; Repo, E. Separation and concentration of rare earth elements from wastewater using electrodialysis technology. *Sep. Purif. Technol.* **2021**, *254*, 117442. [CrossRef]
16. Laurino, J.P. The Extraction and Recovery of Rare Earth Elements from Phosphate Using PX-107 and Chelok®Polymers. 2015. Available online: http://www.fipr.state.fl.us (accessed on 19 January 2023).
17. Elbashier, E.; Mussa, A.; Hafiz, M.; Hawari, A.H. Recovery of rare earth elements from waste streams using membrane processes: An overview. *Hydrometallurgy* **2021**, *204*, 105706. [CrossRef]
18. Larochelle, T.; Noble, A.; Strickland, K.; Ahn, A.; Ziemkiewicz, P.; Constant, J.; Hoffman, D.; Glascock, C. Recovery of Rare Earth Element from Acid Mine Drainage Using Organo-Phosphorus Extractants and Ionic Liquids. *Minerals* **2022**, *12*, 1337. [CrossRef]
19. Chen, B.; He, M.; Zhang, H.; Jiang, Z.; Hu, B. Chromatographic Techniques for Rare Earth Elements Analysis. *Phys. Sci. Rev.* **2017**, *2*, 20160057. [CrossRef]
20. Chen, Y.; Ning, S.; Zhong, Y.; Li, Z.; Wang, J.; Chen, L.; Yin, X.; Fujita, T.; Wei, Y. Study on highly efficient separation of zirconium from scandium with TODGA-modified macroporous silica-polymer based resin. *Sep. Purif. Technol.* **2023**, *305*, 122499. [CrossRef]
21. Analytical Grade Ion Exchange Resins Sample Preparation Specialty Ion Exchange Resins Extraction Chromatographic Resins EXTRACTION CHROMATOGRAPHY Technical Documentation-All Resins. Available online: https://www.triskem-international.com/scripts/files/6454d4deef8fc4.36986672/techdoc_all_resins_0423_website.pdf (accessed on 19 August 2023).
22. Huff, E.A.; Huff, D.R. Tru-Spec and Re-Spec Chromatography-Basic Studies and Applications. In Proceedings of the 34th ORNL/DOE Conference on Analytical Chemistry in Energy Technology, Gatlinburg, TN, USA, 5–7 October 1933.
23. Esser, B.K.; Volpe, A.; Kenneally, J.M.; Smith, D.K. Preconcentration and purification of rare earth elements in natural waters using silica-immobilized 8-hydroxyquinoline and a supported organophosphorus extractant. *Anal. Chem.* **1994**, *66*, 1736–1742. [CrossRef]
24. Wei, Y.; Kumagai, M.; Takashima, Y.; Modolo, G.; Odoj, R. Studies on the separation of minor actinides from high-level wastes by extraction chromatography using novel silica-based extraction resins. *Nucl. Technol.* **2000**, *132*, 413–423. [CrossRef]
25. Nave, S.; Modolo, G.; Madic, C.; Testard, F. Aggregation properties of N,N,N1,N1-Tetraoctyl-3-oxapentanediamide (TODGA) in n-dodecane. *Solvent Extr. Ion Exch.* **2004**, *22*, 527–551. [CrossRef]
26. Husain, M.; Ansari, S.; Mohapatra, P.; Gupta, R.; Parmar, V.; Manchanda, V. Extraction chromatography of lanthanides using N,N,N′,N′-tetraoctyl diglycolamide (TODGA) as the stationary phase. *Desalination* **2008**, *229*, 294–301. [CrossRef]
27. Pourmand, A.; Dauphas, N. Distribution coefficients of 60 elements on TODGA resin: Application to Ca, Lu, Hf, U and Th isotope geochemistry. *Talanta* **2010**, *81*, 741–753. [CrossRef]
28. Baba, Y.; Kubota, F.; Kamiya, N.; Goto, M. Recent Advances in Extraction and Separation of Rare-Earth Metals Using Ionic Liquids. *J. Chem. Eng. Jpn.* **2011**, *44*, 679–685. [CrossRef]
29. Mondal, S.; Ghar, A.; Satpati, A.; Sinharoy, P.; Singh, D.; Sharma, J.; Sreenivas, T.; Kain, V. Recovery of rare earth elements from coal fly ash using TEHDGA impregnated resin. *Hydrometallurgy* **2019**, *185*, 93–101. [CrossRef]
30. Horwitz, E.P.; McAlister, D.R.; Bond, A.H.; Barrans, R.E. Novel extraction of chromatographic resins based on tetraalkyldiglycolamides: Characterization and potential applications. *Solvent Extr. Ion Exch.* **2005**, *23*, 319–344. [CrossRef]
31. Turanov, A.N.; Karandashev, V.K.; Yarkevich, A.N. Extraction of REEs(III), U(VI), and Th(IV) from nitric acid solutions with carbamoylmethylphosphine oxides in the presence of an ionic liquid. *Radiochemistry* **2013**, *55*, 382–387. [CrossRef]
32. Agafonova-Moroz, M.S.; Krasnikov, L.V.; Mishina, N.E.; Shadrin, A.Y.; Shmidt, O.V. Extraction of Eu and Am with extractants based on carbamoyl phosphine oxide (CMPO). *Radiochemistry* **2009**, *51*, 403–405. [CrossRef]
33. Papp, I.; Vajda, N.; Happel, S. An improved rapid method for the determination of actinides in water. *J. Radioanal. Nucl. Chem.* **2022**, *331*, 3835–3846. [CrossRef]
34. Larenkov, A.A.; Makichyan, A.G.; Iatsenko, V.N. Separation of44sc from44ti in the context of a generator system for radiopharmaceutical purposes with the example of [44sc]sc-psma-617 and [44sc]sc-psma-i&t synthesis. *Molecules* **2021**, *26*, 6371. [CrossRef]
35. Zoleta, J.B.; Itao, G.B.; Resabal, V.J.T.; Lubguban, A.A.; Corpuz, R.D.; Ito, M.; Hiroyoshi, N.; Tabelin, C.B. Improved pyrolysis behavior of ammonium polyphosphate-melamine-expandable (APP-MEL-EG) intumescent fire retardant coating system using ceria and dolomite as additives for I-beam steel application. *Heliyon* **2019**, *6*, e03119. [CrossRef]
36. Agbovi, H.K.; Wilson, L.D. Adsorption processes in biopolymer systems: Fundamentals to practical applications. In *Natural Polymers-Based Green Adsorbents for Water Treatment*; Elsevier: Amsterdam, The Netherlands, 2021; pp. 1–51. [CrossRef]
37. Fang, J.; Xuan, Y.; Li, Q. Preparation of polystyrene spheres in different particle sizes and assembly of the PS colloidal crystals. *Sci. China Technol. Sci.* **2010**, *53*, 3088–3093. [CrossRef]
38. Tabelin, C.B.; Veerawattananun, S.; Ito, M.; Hiroyoshi, N.; Igarashi, T. Pyrite oxidation in the presence of hematite and alumina: I. Batch leaching experiments and kinetic modeling calculations. *Sci. Total. Environ.* **2017**, *580*, 687–698. [CrossRef] [PubMed]

39. Annam, S.; Rao, C.B.; Sivaraman, N.; Sivaramakrishna, A.; Vijayakrishna, K. Carbamoylmethylphosphine oxide functionalised porous crosslinked polymers towards sequential separation of uranium (VI) and thorium (IV). *React. Funct. Polym.* **2018**, *131*, 203–210. [CrossRef]
40. Cho, Y.; Ivanisevic, A. Covalent attachment of TAT peptides and thiolated alkyl molecules on GaAs surfaces. *J. Phys. Chem. B* **2005**, *109*, 12731–12737. [CrossRef]
41. Patel, M.A.; Luo, F.; Khoshi, M.R.; Rabie, E.; Zhang, Q.; Flach, C.R.; Mendelsohn, R.; Garfunkel, E.; Szostak, M.; He, H. P-Doped Porous Carbon as Metal Free Catalysts for Selective Aerobic Oxidation with an Unexpected Mechanism. *ACS Nano* **2016**, *10*, 2305–2315. [CrossRef]
42. Popat, K.C.; Swan, E.E.L.; Desai, T.A. Modeling of RGDC film parameters using X-ray photoelectron spectroscopy. *Langmuir* **2005**, *21*, 7061–7065. [CrossRef] [PubMed]
43. Kehrer, M.; Duchoslav, J.; Hinterreiter, A.; Cobet, M.; Mehic, A.; Stehrer, T.; Stifter, D. XPS investigation on the reactivity of surface imine groups with TFAA. *Plasma Process. Polym.* **2019**, *16*, 1800160. [CrossRef]
44. Friedman, A.K.; Shi, W.; Losovyj, Y.; Siedle, A.R.; Baker, L.A. Mapping Microscale Chemical Heterogeneity in Nafion Membranes with X-ray Photoelectron Spectroscopy. *J. Electrochem. Soc.* **2018**, *165*, H733–H741. [CrossRef]
45. Sydorchuk, V.; Poddubnaya, O.; Tsyba, M.; Zakutevskyy, O.; Khyzhun, O.; Khalameida, S.; Puziy, A. Photocatalytic degradation of dyes using phosphorus-containing activated carbons. *Appl. Surf. Sci.* **2020**, *535*, 147667. [CrossRef]
46. Tabelin, C.B.; Igarashi, T.; Yoneda, T.; Tamamura, S. Utilization of natural and artificial adsorbents in the mitigation of arsenic leached from hydrothermally altered rock. *Eng. Geol.* **2013**, *156*, 58–67. [CrossRef]
47. Tabelin, C.B.; Igarashi, T.; Arima, T.; Sato, D.; Tatsuhara, T.; Tamoto, S. Characterization and evaluation of arsenic and boron adsorption onto natural geologic materials, and their application in the disposal of excavated altered rock. *Geoderma* **2014**, *213*, 163–172. [CrossRef]
48. Opiso, E.M.; Tabelin, C.B.; Ramos, L.M.; Gabiana, L.J.R.; Banda, M.H.T.; Delfinado, J.R.Y.; Orbecido, A.H.; Zoleta, J.B.; Park, I.; Arima, T.; et al. Development of a three-step approach to repurpose nickel-laterite mining waste into magnetite adsorbents for As(III) and As(V) removal: Synthesis, characterization and adsorption studies. *J. Environ. Chem. Eng.* **2023**, *11*, 108992. [CrossRef]
49. Pearson, R.G. Physical and Inorganic Chemistry Hard and Soft Acids and Bases. 1963. Available online: https://pubs.acs.org/sharingguidelines (accessed on 5 September 2023).
50. Parr, R.G.; Pearson, R.G. Absolute Hardness: Companion Parameter to Absolute Electronegativity. *J. Am. Chem. Soc.* **1983**, *105*, 7512–7516. [CrossRef]
51. Lee, Y.-R.; Yu, K.; Ravi, S.; Ahn, W.-S. Selective Adsorption of Rare Earth Elements over Functionalized Cr-MIL-101. *ACS Appl. Mater. Interfaces* **2018**, *10*, 23918–23927. [CrossRef] [PubMed]
52. Ansari, S.; Pathak, P.; Mohapatra, P.K.; Manchanda, V.K. Chemistry of diglycolamides: Promising extractants for actinide partitioning. *Chem. Rev.* **2012**, *112*, 1751–1772. [CrossRef]